ROYAL SOCIETY OF CHEMISTRY

EDGE ARTICLE

A dual-fluorophore sensor approach for ratiometric fluorescence imaging of potassium in living cells†

Zeming Wang,[a] Tyler C. Detomasi [ID][a] and Christopher J. Chang [ID] *[abc]

Potassium is the most abundant intracellular metal in the body, playing vital roles in regulating intracellular fluid volume, nutrient transport, and cell-to-cell communication through nerve and muscle contraction. On the other hand, aberrant alterations in K$^+$ homeostasis contribute to a diverse array of diseases spanning cardiovascular and neurological disorders to diabetes to kidney disease to cancer. There is an unmet need for studies of K$^+$ physiology and pathology owing to the large differences in intracellular *versus* extracellular K$^+$ concentrations ($[K^+]_{intra}$ = 150 mM, $[K^+]_{extra}$ = 3–5 mM). With a relative dearth of methods to reliably measure dynamic changes in intracellular K$^+$ in biological specimens that meet the dual challenges of low affinity and high selectivity for K$^+$, particularly over Na$^+$, currently available fluorescent K$^+$ sensors are largely optimized with high-affinity receptors that are more amenable for extracellular K$^+$ detection. We report the design, synthesis, and biological evaluation of Ratiometric Potassium Sensor 1 (**RPS-1**), a dual-fluorophore sensor that enables ratiometric fluorescence imaging of intracellular potassium in living systems. **RPS-1** links a potassium-responsive fluorescent sensor fragment (**PS525**) with a low-affinity, high-selectivity crown ether receptor for K$^+$ to a potassium-insensitive reference fluorophore (**Coumarin 343**) as an internal calibration standard through ester bonds. Upon intracellular delivery, esterase-directed cleavage splits these two dyes into separate fragments to enable ratiometric detection of K$^+$. **RPS-1** responds to K$^+$ in aqueous buffer with high selectivity over competing metal ions and is sensitive to potassium ions at steady-state intracellular levels and can respond to decreases or increases from that basal set point. Moreover, **RPS-1** was applied for comparative screening of K$^+$ pools across a panel of different cancer cell lines, revealing elevations in basal intracellular K$^+$ in metastatic breast cancer cell lines *vs.* normal breast cells. This work provides a unique chemical tool for the study of intracellular potassium dynamics and a starting point for the design of other ratiometric fluorescent sensors based on two-fluorophore approaches that do not rely on FRET or related energy transfer designs.

Introduction

All cells in all living organisms require potassium,[1,2] where the abundant K$^+$ cation regulates cellular osmolality, nutrient status, and membrane potential,[3–5] contributing to physiological processes including neuron firing, muscle contraction,[6,7] and hormone regulation.[8–10] Cellular potassium homeostasis is maintained by an intricate network of membrane K$^+$ channels and pumps, giving physiological K$^+$ concentrations ranging from approximately 3–5 mM extracellularly to 150 mM intracellularly.[11] Aberrant elevations or depletions of intracellular K$^+$ from these tightly regulated set points, caused largely by

malfunction of K$^+$ channels or pumps, can contribute to serious diseases that range from neurodegeneration and epilepsy to kidney failure to diabetes to arrhythmia and heart disorders to cancer.[12,13] In one example, a growing body of literature connects K$^+$ channels to cancer through cell motility, which is critical to tumor growth and metastasis.[12–21] However, most of these studies have focused on correlations of aberrant expression of K$^+$ channels in various types of cancer and suggest a relationship between altered intracellular K$^+$ level and cell apoptosis,[16,22,23] with limited information on direct measurements of K$^+$ pools themselves.

These foregoing considerations motivate the development of chemical tools that can enable detection of K$^+$ pools in living biological specimens with higher spatial and temporal resolution compared to conventional methods of detection such as K$^+$-selective microelectrodes and patch clamp techniques.[24,25] Notably, recent years have also seen advances in the development of genetically encoded potassium probes and nanosensors.[26–31] In this context, small-molecule fluorescent sensors

[a]*Department of Chemistry, University of California, Berkeley, CA 94720, USA. E-mail: chrischang@berkeley.edu*

[b]*Department of Molecular and Cell Biology, University of California, Berkeley, CA 94720, USA*

[c]*Helen Wills Neuroscience Institute, University of California, Berkeley, CA 94720, USA*

† Electronic supplementary information (ESI) available. See DOI: 10.1039/d0sc03844j

offer an attractive approach to meet this goal, as they are valued as non-invasive, high signal-to-noise reagents that can accurately map a variety of biological analytes, particularly metal ions.[32–37] Despite notable advances in the development of small-molecule fluorescent sensors for potassium,[38–45] imaging intracellular K⁺ in biological samples with high selectivity over Na⁺ remains a significant and insufficiently solved challenge, owing in large part to high resting K⁺ concentrations within the cell (150 mM), which requires a low-affinity molecular recognition element that still achieves high K⁺ selectivity. Pioneering work by Tsien and Minta on the first potassium probe, potassium benzofuran isophthalic acid (PBFI), offered an important early solution to this problem, but PBFI is limited by slow cellular uptake kinetics due to its high molecular weight and need for UV excitation, which can trigger background autofluorescence and sample photodamage.[46] Likewise, He and colleagues developed a high-affinity fluorescent K⁺ sensor based on a tri-aza-cryptand potassium receptor,[38] and Verkman and other research teams have successfully developed several useful sensors for monitoring extracellular K⁺, including stimulated K⁺ release, based on this ionophore.[47–50] Specifically, the Verkman laboratory has demonstrated visualizing K⁺ waves in brain cortex using a K⁺ indicator.[51] K⁺ sensors have also been developed using native and engineered nucleic acid G-quadruplex binding motifs.[39,40,52,53] As such, the vast majority of available fluorescent K⁺ sensors for biological use achieve selectivity of K⁺ over Na⁺ by high-affinity means. However, the tight-binding nature of these probes does not allow for a dynamic range of

detection of K⁺ in the cytosol without saturation, limiting their utility for studies of intracellular K⁺ dynamics (Fig. 1).

In addition, currently available small-molecule fluorescent K⁺ sensors are limited to intensity-based responses. In the best case scenario, such turn-on fluorescence potassium probes can detect dynamic K⁺ fluxes within the same cell population before and after a stimulation event, but comparing relative K⁺ levels across different biological samples can be complicated. Proper comparisons can be hindered by variations in: intracellular delivery, uptake, and retention of probes among cell types; sample thickness and other heterogeneities, and both excitation and emission light intensity and power dependency. These issues can be mitigated by ratiometric fluorescence imaging, which enables calibration by an internal standard.[54] Along these lines, we have recently reported activity-based sensing probes for iron[55] (FRET Iron Probe-1, **FIP-1**) and copper[56] (FRET Copper Probe-1, **FCP-1**), which feature ratiometric fluorescence detection using a fluorescence resonance energy transfer (FRET) strategy.

Here we report the design, synthesis, and biological evaluation of a first-generation ratiometric fluorescent sensor for K⁺ detection, termed Ratiometric Potassium Sensor-1 (**RPS-1**). **RPS-1** is composed of a dual-fluorophore system that combines a K⁺-responsive rhodol moiety (Potassium Sensor 525, **PS525**) and a standard fluorophore (**Coumarin 343**) for more suited sensing to intracellular [K⁺] levels in the 150 mM range with internal self-calibration. Unlike previously reported **FIP-1** and **FCP-1** indicators that rely on FRET, the two fluorophores in **RPS-1** are spectrally distinct and are not designed to undergo internal energy transfer. Instead, **RPS-1** utilizes ester linkers that can be cleaved by intracellular esterases to detach the K⁺-responsive fluorophore from its internal standard and trap both dyes inside the cell in their carboxylate forms, an approach inspired by previous work by Woodroofe and Lippard on ratiometric zinc sensors.[57] As a key design feature to tailor its use for intracellular K⁺ detection, the **PS525** portion of **RPS-1** utilizes a lariat-modified crown ether to achieve a K_d value more in line with intracellular K⁺ levels (Fig. 1).[42,58,59] Indeed, despite its low affinity for K⁺, **RPS-1** shows sufficient selectivity for K⁺ over competing biologically relevant metal ions, including Na⁺, and is able to monitor intracellular K⁺ fluxes. Moreover, because ratiometric calibration minimizes interference arising from analyte-independent phenomena such as sample thickness, heterogeneity, variations in light intensity, and dye loading, **RPS-1** enables a rapid readout of K⁺ levels among different cell lines that can be corroborated by ICP-MS. Interestingly, data from these independent measurements reveal that select types of breast cancer cells possess elevated concentrations of K⁺ relative to normal breast cell counterparts. In addition to providing a unique chemical tool for interrogating intracellular K⁺ dynamics, this chemical modification strategy of converting a turn-on probe to a ratiometric probe is broadly applicable to a variety of fluorescent probes for different analytes provided each fluorophore has a non-overlapping emission spectrum. Taken together, **RPS-1** provides key advances in terms of visible wavelength excitation and emission to
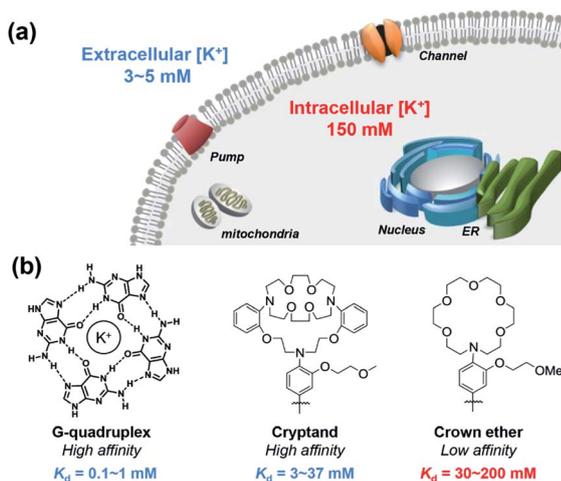
Fig. 1 Design considerations of extracellular and intracellular potassium pools and potassium-binding receptors for the development of Ratiometric Potassium Sensor-1 (**RPS-1**). (a) Comparison of extracellular and intracellular potassium pools showing higher resting levels of K⁺ inside *versus* outside the cell. (b) Comparison of high-affinity G-quadruplex and cryptand receptors tailored for extracellular K⁺ binding *versus* lariat crown ether receptors that are more amenable for intracellular K⁺ binding. The K_d values of both G-quadruplex- and cryptand-based receptors are well-matched with extracellular [K⁺] levels in the 3–5 mM range, whereas the weaker-binding lariat crown ether ionophores are more suited sensing to intracellular [K⁺] levels in the 150 mM range.

minimize background autofluorescence and photodamage to biological samples, a low-affinity K⁺ receptor that retains high selectivity over Na⁺ to better match intracellular [K⁺] levels in the 150 mM range, and a ratiometric response to enable internal self-calibration.

Results and discussion

Design of Ratiometric Potassium Sensor-1 (RPS-1), a dual-fluorophore probe for ratiometric potassium detection

To develop a ratiometric sensing platform for potassium tailored for intracellular use, we envisioned a dual-fluorophore system with two dyes, one being potassium-sensitive and one being potassium-insensitive, which could be delivered in a 1 : 1 ratio to cells. In principle, the potassium-sensitive moiety would possess a low-affinity receptor to better match the high levels of resting intracellular K⁺ pools in the 150 mM range and respond by an intensity-based turn-on response, whereas the potassium-insensitive dye would exhibit a distinct spectral excitation and emission from the potassium sensor for internal calibration. We chose **Coumarin 343** as the internal standard fluorophore owing to its lack of a fluorescence response to K⁺, and we designed and synthesized the new potassium-responsive dye Potassium Sensor 525 (**PS525**) for the other portion of the sensor (Scheme 1a). **Coumarin 343** is coupled to **PS525** *via* two ester-based linkers to yield **RPS-1** (Scheme 1b). After **RPS-1** is delivered into the cells, cellular esterases will cleave the ester bonds to give two separate fluorophores, **PS525** (K⁺-responsive) and **Coumarin 343** (K⁺-insensitive), in a 1 : 1 ratio (Scheme 1c). After cleavage, both fluorophores are cell-trappable due to their negatively charged carboxylate groups. As such, the ratio of respective emission profiles for **PS525** and **Coumarin 343** can determine a readout of intracellular K⁺ concentrations.

Synthesis and characterization of the K⁺-responsive turn-on probe Potassium Sensor 525 (PS525)

As our design of **RPS-1** is comprised of a K⁺-responsive fluorescent moiety linked to an internal dye standard for ratiometric calibration, we sought to prepare a new turn-on fluorescent sensor that responds selectively to K⁺ in the high intracellular [K⁺] range of 150 mM. To achieve this goal, we chose a lariat ether modified aza-crown ether receptor as the K⁺-responsive moiety, as it retains high selectivity for K⁺ over Na⁺ but exhibits a weaker binding affinity for K⁺ compared to cryptand and G-quadruplex moieties (Fig. 1b and 2a). The probe is designed to operate by a standard photoinduced electron transfer (PET) mechanism where the electron-rich amine receptor will quench fluorescence by PET, which is alleviated by binding of the positively charged cation to the receptor.[33,60] We appended this receptor to a rhodol-based structure owing to its spectral separation from **Coumarin 343** and attractive imaging properties, including good optical brightness and photostability in one- and two-photon modes, as well as a balance between hydrophilicity and cell-permeability.[35,61,62]

The synthesis of this K⁺ responsive moiety, Potassium Sensor 525 (**PS525**), is shown in Scheme 2. Lariat ether modified aza-crown ether **1** was synthesized using published procedures[42] and then converted to xanthene **2** through a Vilsmeier–Haack reaction using phosphoryl chloride in *N,N*-dimethylformamide, followed by resorcinol condensation with trifluoroacetic acid as the solvent. Rhodol **3** was synthesized by converting the hydroxyl group on **2** to a triflate group, followed by Buchwald–Hartwig amination to add *tert*-butoxycarbonyl(Boc)-protected piperazine group and worked up with a trace amount of trifluoroacetic acid. Finally, **PS525** was obtained by reacting **3** with methyl 2-bromoacetate, followed by treatment of lithium hydroxide in tetrahydrofuran and water mixture.
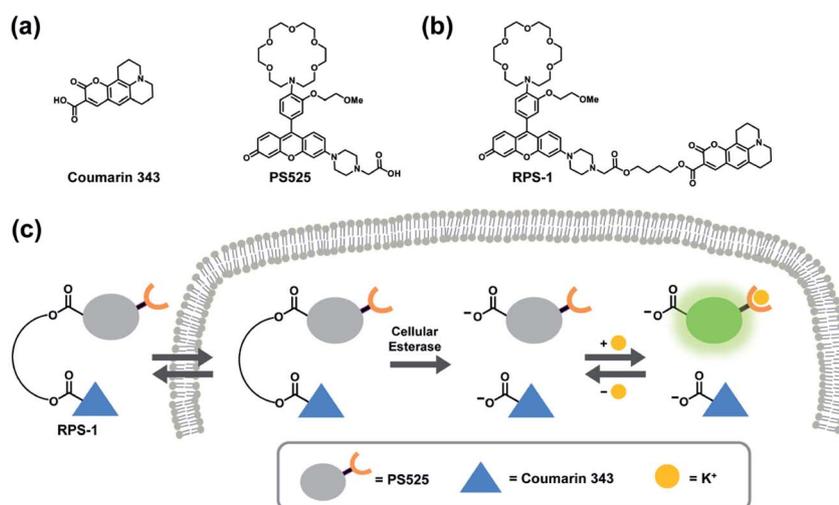
Scheme 1 Design and action of Ratiometric Potassium Sensor-1 (**RPS-1**). (a) Molecular structures of K⁺-insensitive **Coumarin 343** and K⁺-responsive Potassium Sensor 525 (**PS525**) portions to generate (b) **RPS-1**. (c) **RPS-1** is cleaved by intracellular esterases back to **PS525** and **Coumarin 343**, which are both cell-trappable owing to their negatively charged carboxylate motifs. Because **PS525** has a turn-on response to K⁺ whereas **Coumarin 343** is non-responsive to K⁺, ratiometric fluorescence measurements can be made using two-channel imaging and be correlated with changes in K⁺.
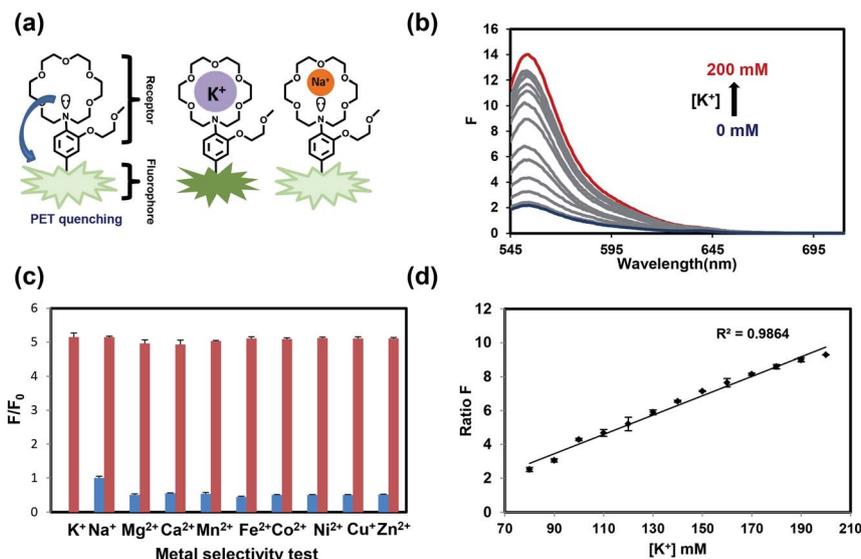
Fig. 2 Turn-on response and potassium selectivity for PS525. (a) Photoinduced electron transfer (PET) sensing and K$^+$/Na$^+$ selectivity mechanism for lariat ether sensor PS525. (b) Fluorescence spectra of 2 μM PS525 in HEPES buffer (pH 7.4) containing [K$^+$] at 0, 5, 10, 20, 30, 40, 50, 70, 90, 110, 130, 150, 200 mM. The blue trace is at 0 mM K$^+$ and red trace is at 200 mM K$^+$. Excitation was provided at 525 nm. (c) Fluorescence intensity changes of PS525 in the presence of competing biological metal ions at the physiological concentrations with (red) or without (blue) K$^+$: K$^+$ (150 mM), Na$^+$ (5.0 mM), Mg^{2+} (2.0 mM), Ca^{2+} (2.0 mM), Mn^{2+} (10 μM), Fe^{2+} (10 μM), Co^{2+} (10 μM), Ni^{2+} (10 μM), Cu^{2+} (10 μM), Zn^{2+} (10 μM). (d) Response of the ratio of the fluorescence intensity of PS525 and Coumarin 343 to physiologically relevant K$^+$ levels. 5 μM PS525 and Coumarin 343 (1 : 1) in HEPES buffer (50 mM, pH 7.4) was used for measurement. Peak intensity value of PS525 (552 nm) and Coumarin 343 (490 nm) was obtained to calculate ratio intensity. Error bars denote SEM, $n = 3$.

We evaluated the optical properties of PS525 in aqueous solution buffered to physiological pH (50 mM HEPES, pH 7.4). PS525 shows a maximum absorption peak at 525 nm with calculated absorption coefficients of $\varepsilon = 61\,100\ \mathrm{M}^{-1}\ \mathrm{cm}^{-1}$ and $\varepsilon = 65\,000\ \mathrm{M}^{-1}\ \mathrm{cm}^{-1}$ in the presence of 0 and 200 mM of K$^+$, respectively (Fig. S2†). When exposed to K$^+$, PS525 shows a 7-fold turn-on increase in fluorescence emission centered at 552 nm (Fig. 2b), with a quantum yield increase from 0.03 in the absence of K$^+$ to 0.15 in the presence of K$^+$ (Fig. S2†). The K_d value of the probe was calculated to be 137 mM based on the K$^+$ titration response using a Benesi–Hildebrand plot (Fig. S1†), which is well-matched with intracellular [K$^+$] in the 150 mM range.
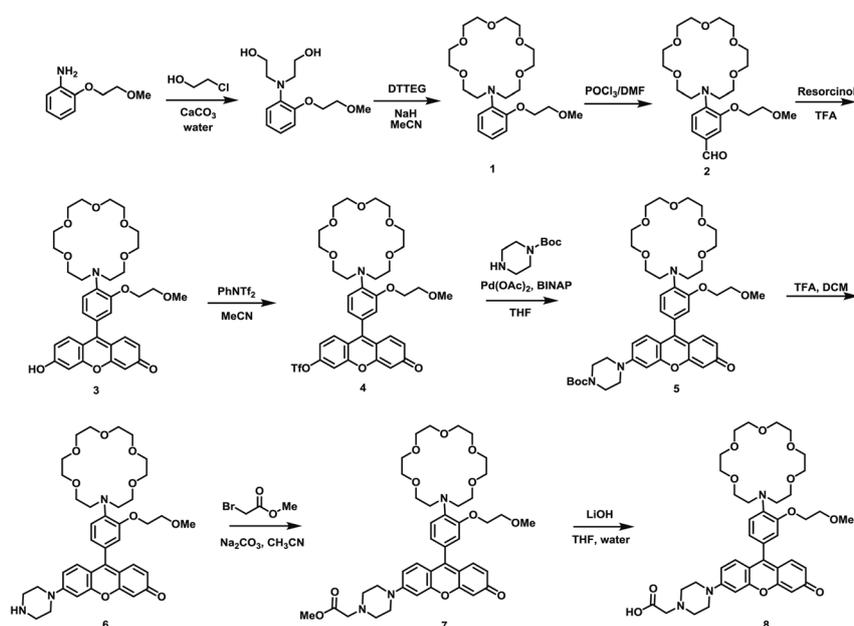
Scheme 2 Synthesis of PS525.

We next tested the metal selectivity of **PS525** for K$^+$ compared to a panel of biologically relevant alkali, alkaline earth, and transition metals (Fig. 2c). Notably, even with its low affinity for K$^+$, **PS525** showed a greater than five-fold selectivity for K$^+$ over Na$^+$ at relevant intracellular levels, presaging that it possesses adequate sensitivity and selectivity for downstream biological applications. We then tested the sensitivity of the ratio responsiveness of **PS525** and **Coumarin 343** to the K$^+$ level around intracellular K$^+$ concentration (140 mM) (Fig. 2d). Within the range of 80 mM to 120 mM, linear regression analysis was performed to calculate limit of detection at 5.8 mM. Additionally, the pH sensitivity test of both **PS525** and **Coumarin 343** demonstrated their usability under physiological pH (Fig. S3†).

Synthesis of Ratiometric Potassium Sensor-1 (RPS-1) from PS525 and Coumarin 343 dyes and demonstration of ratiometric fluorescence imaging of K$^+$ levels in living cells

After establishing that **PS525** is a selective and sensitive fluorescent K$^+$-sensing dye unit, we synthesized **RPS-1** through esterification of **PS525** with a previously reported coumarin synthon[63] using 2-(3H-[1,2,3]triazolo[4,5-b]pyridine-3-yl)-1,1,3,3-tetramethyluronium tetrafluoroborate (TATU) as a carboxylate activator (Fig. 3a). We tested the fluorescence response and esterase-catalyzed hydrolysis of **RPS-1** (Fig. S4 and S5†). We next applied **RPS-1** for ratiometric fluorescence imaging of intracellular K$^+$ pools with confocal microscopy, given the ability of the **PS525** sensing unit to respond selectively to K$^+$ levels at biologically relevant concentrations in aqueous buffer *in vitro*. We note that the K$^+$-insensitive **Coumarin 343** piece has a quantum yield of 0.02, which is comparable to the **PS525** portion, but is excited at a separate 458 nm wavelength (Fig. S2†). HeLa cells were first incubated with 10 µM **RPS-1** before imaging to ensure probe uptake and esterase cleavage. Dual-color confocal microscopy images were acquired using 458 nm excitation of the **Coumarin 343** unit (blue channel) and 514 nm excitation of the **PS525** unit (green channel). A ratio image was then obtained using these two channels (green channel/blue channel, Fig. 3b). To assess whether **RPS-1** can respond to changes in intracellular K$^+$ changes through its **PS525** unit, HeLa cells were then treated with 5 µM valinomycin, a compound known to chelate and transport potassium selectively through membranes and deplete intracellular pools of K$^+$. Confocal images from both channels were taken at 0, 5, 15, 30, 45, 60 min after valinomycin addition and compared with a vehicle control. We observed a clear decrease in green/blue ratio intensities in the HeLa cells stimulated by valinomycin compared to the cells in the vehicle control group (Fig. 3c). Furthermore, we confirmed that cells treated with valinomycin indeed have decreased levels of intracellular K$^+$ through inductively coupled plasma mass spectrometry measurements (ICP-MS; Fig. S5†). These data suggest that **RPS-1** can respond to dynamic changes in intracellular K$^+$ pools and is capable of monitoring decreases in [K$^+$] from basal levels. Moreover, the dual-fluorophore ratio from the vehicle control remains stable throughout the time course of the experiment, consistent with the design in which the two dye
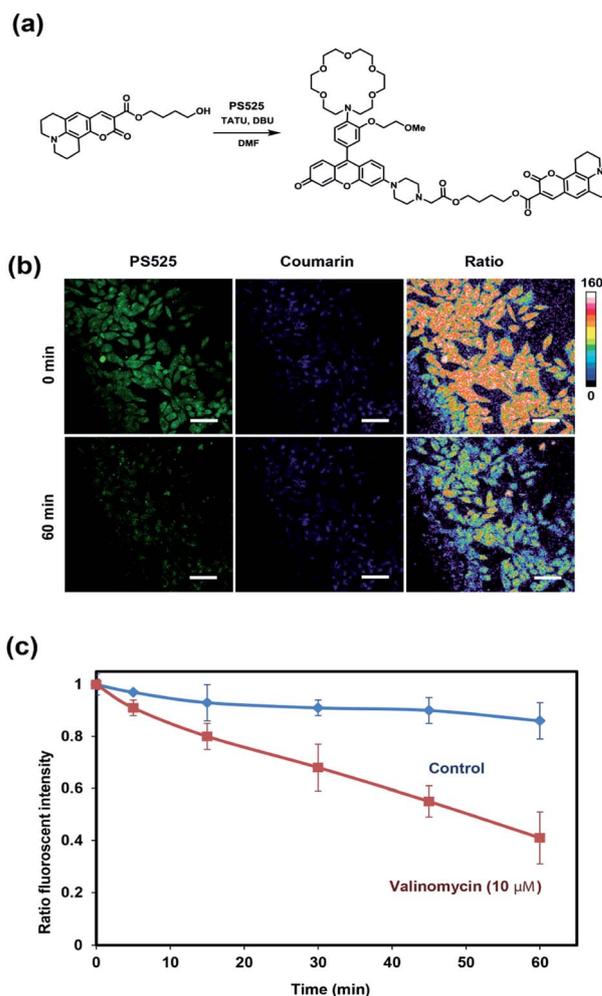

Fig. 3 (a) Synthesis of **RPS-1** and ratiometric imaging of intracellular K$^+$ pools using **RPS-1**. (b) Time-dependent ratiometric fluorescence imaging with **RPS-1** enables monitoring of depletion of intracellular K$^+$ pools in live HeLa cells treated with 5 µM valinomycin for 1 h. The green channel shows emission from the **PS525** chromophore with 514 nm excitation, and the blue channel shows emission from the **Coumarin 343** chromophore with 458 nm excitation. Fluorescence ratio images from the two channels were constructed from ImageJ. (c) Average fluorescence intensity ratios from multiple biological replicates plotted as measured and analysed by ImageJ. Decreases of intracellular K$^+$ levels upon valinomycin stimulation are clearly shown by fluorescence ratio changes (red trace) relative to vehicle control (blue trace). Error bars denote SEM for mean green/blue ratios, $n = 3$. Scale bar = 25 µm.

components are delivered and trapped upon esterase cleavage. Finally, cell viability was measured through propidium iodide staining and was not significantly different with valinomycin and/or **RPS-1** treatments over the course of the experiment (Fig. S6†).

We next tested the ability of **RPS-1** to detect increases in intracellular K$^+$ levels upon stimulation. HT29 cells are known to selectively express significantly higher levels of the human ether-à-go-go-related gene (HERG) potassium channel relative to other cancer cell lines such as HeLa and A549.[64,65] We treated HT29 cells with astemizole, a known HERG potassium channel blocker, to enable expansion of intracellular K$^+$ pools.[66] We first
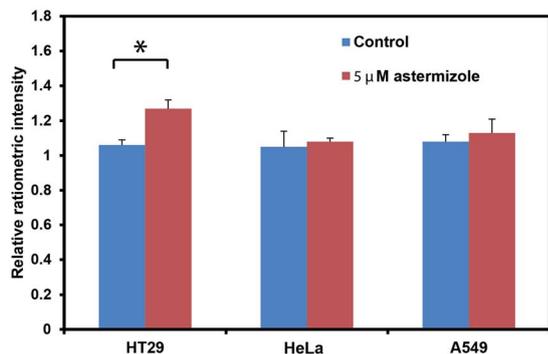
Fig. 4 Application of RPS-1 to assay astemizole-induced K^+ influx across a variety of cell lines. Data shown for HT29 cancer cells compared to HeLa and A549 cells under basal conditions and after treatment with 5 μM asterizole for 1 h. Mean Green/Blue ratio was obtained for each cell line; error bars denote SEM, $n = 3$. Statistical significance was assessed by calculating the p-value using one-way ANOVA with Bonferroni correction in R, $*p < 0.05$.
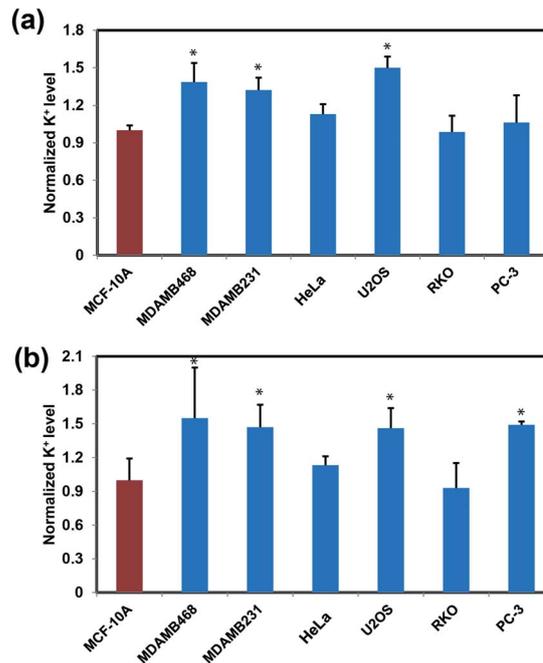

Fig. 5 Profiling relative resting intracellular K^+ levels in various cancer and non-cancerous (MCF-10A) cell lines by RPS-1 and ICP-MS. Data given for (a) RPS-1 and (b) ICP-MS. Average fluorescence intensity ratios are measured using ImageJ. Error bars denote SEM, $n = 3$. Statistical significance was assessed by calculating the p-value using one-way ANOVA with Bonferroni correction in R, $*p < 0.05$.

incubated all three cell types with 10 μM **RPS-1** for 3 hours, followed by media exchange and treatment with 5 μM astemizole and 30 mM K^+ or with vehicle control in HEPES buffer for 1 hour. We observed an increase in the ratio of green/blue fluorescence in the HT29 cells compared to vehicle control and Hela and A549 cell lines (Fig. 4). The astermizole-induced increases in intracellular K^+ levels were verified by ICP-MS (Fig. S5†). Taken together, these data establish that **RPS-1** is indeed able to visualize both increases and decreases in intracellular K^+ levels by ratiometric fluorescence imaging.

RPS-1 enables profiling of intracellular K^+ levels across a panel of cancer cell lines

After establishing that **RPS-1** is capable of monitoring dynamic changes in intracellular K^+ levels upon external stimulation, we sought to expand applications of **RPS-1** to profiling relative intracellular K^+ levels across different cell types. We became interested in comparative screening of K^+ levels between cancer and non-cancer cell models, as many types of tumors are known to exhibit elevated K^+ channel expression and elevated K^+ has been observed in some cases.[18,21,67] We turned our attention to comparing K^+ levels in two different types of metastatic breast cancer cell lines, MDA-MB-468 and MDA-MB-231, relative to a normal breast cancer cell control line MCF-10A. Given the ability of **RPS-1** to reliably measure the relative intracellular K^+ level in multiple types of cell lines, we also screened other cancer cell lines, including U2OS (bone), RKO (colon), and PC-3 (prostate), using HeLa as a comparison. Interestingly, **RPS-1** imaging reveals that the breast cancer cell lines MDA-MB-468 and MDA-MB-231 possess higher basal levels of K^+ compared to the normal breast cell line MCF-10A (Fig. 5). We speculate that the expansion of K^+ pools is due to higher proliferation needs for metastatic tumor cells *versus* normal ones. In addition, PC-3 and U2OS lines also exhibit higher resting levels of K^+ over RKO and HeLa, showing that different cell types can indeed possess different basal K^+ pools. Moreover, ICP-MS

measurements of bulk intracellular K^+ levels validate the **RPS-1** assay by providing an independent measure of potassium (Fig. 5 and S8†).

Concluding remarks

To summarize, we have presented the design, synthesis, characterization, and biological applications of **RPS-1**, a first-generation chemical probe for ratiometric imaging of intracellular K^+ pools. **RPS-1** features a dual-fluorophore approach to ratiometric potassium detection where the two fluorophores operate independently to provide a potassium-sensitive response in one dye with internal calibration from the other dye. **RPS-1** is composed of two units: **PS525** as a turn-on K^+-responsive fluorophore with a lariat crown ether receptor tailored to selective but low-affinity K^+ binding, and **Coumarin 343** as a K^+-insensitive fluorophore. When joined by ester linkages in the full **RPS-1** probe, both components are taken up, released, and trapped in cells after cleavage by intracellular esterases. Through the **PS525** unit, **RPS-1** can sensitively and specifically respond to intracellular K^+ as well as report dynamic changes in K^+ levels upon stimulation with an external input. Compared to previous potassium probes such as PBFI, which requires high-energy UV excitation, visible light excitation of **RPS-1** through the **PS525** chromophore minimizes background autofluorescence and photodamage. Moreover, due to its ratiometric response **RPS-1** can be used to profile basal intracellular K^+ pools across a variety of different cell lines, revealing

that breast cancer cells possess higher resting levels than a non-cancerous counterpart. We anticipate that **RPS-1** and related fluorescent probes will be of value in providing foundational information about K^+ physiology and pathology owing to the broad importance of this abundant metal in biology, as well as promote further investigations into design strategies for ratiometric detection of metals and other important biological analytes.

Experimental section

General methods

Reactions using moisture- or air-sensitive reagents were carried out in flame-dried glassware in an inert atmosphere of N_2. Solvent was passed over activated alumina and stored over activated 3 Å molecular sieves before use when dry solvent was required. All other commercially purchased chemicals were used as received (without further purification). SiliCycle 60 F254 silica gel pre-coated sheets (0.25 mm thick) were used for analytical thin layer chromatography and visualized by fluorescence quenching under UV light. Silica gel P60 (SiliCycle) was used for column chromatography. ^{1}H and ^{13}C NMR NMR spectra were collected at 298 K in $CDCl_3$ or CD_3OD (Cambridge Isotope Laboratories, Cambridge, MA) at 25 °C using Bruker AVQ-400, AVB-400, AV-500, or AV-600 instruments at the College of Chemistry NMR Facility at the University of California, Berkeley or using a Bruker 900 at the QB3 Central California 900 MHz NMR Facility. All chemical shifts are reported in the standard notation of δ parts per million relative to the residual solvent peak at 7.26 ($CDCl_3$) or 3.31 (CD_3OD) for ^{1}H and 77.16 ($CDCl_3$) or 49.00 (CD_3OD) for ^{13}C as an internal reference. Splitting patterns are indicated as follows: br, broad; s, singlet; d, doublet; t, triplet; m, multiplet; dd, doublet of doublets. Low-resolution electrospray mass spectral analyses were carried out using LC-MS (Agilent Technology 6130, Quadrupole LC/MS and Advion Expression-L Compact Mass Spectrometer). High-resolution mass spectral analyses (ESI-MS) were carried out at the College of Chemistry Mass Spectrometry Facility at the University of California, Berkeley. Compound **1** was synthesized using the published procedure.[42] All aqueous solutions were prepared using Milli-Q water, and all spectroscopic experiments were carried out in 50 mM HEPES, pH 7.4, unless otherwise noted. All spectroscopic experiments were prepared using freshly prepared aliquots. Absorption spectra were acquired using a Varian Cary 50 spectrophotometer, and fluorescence spectra were acquired using a Photon Technology International Quanta Master 4 L-format scan spectro-fluorometer equipped with an LPS-220B 75 W xenon lamp and power supply, A-1010B lamp housing with an integrated igniter, switchable 814 photocounting/analog photomultiplier detection unit, and MD5020 motor driver. 1 cm × 1 cm quartz cuvettes (1.4 mL volume, Starna, capped) were used for obtaining absorption and fluorescence spectra. For all fluorescence measurements and K^+ studies, aqueous solutions of KCl (Sigma) were used. For metal selectivity studies, aqueous metal solutions of $MgCl_2 \cdot 4H_2O$ (EMD Millipore), $CaCl_2 \cdot 2H_2O$ (EMD Millipore), $NiCl_2 \cdot 6H_2O$ (Sigma), $ZnCl_2$ (Sigma),

$CuCl_2 \cdot 2H_2O$ (Baker & Adamson), $CoCl_2 \cdot 6H_2O$ (Sigma), $MgCl_2 \cdot 6H_2O$ (Sigma), NaCl (Sigma), and $FeCl_2$ (Sigma) were used.

Synthesis of RPS-1

4-(1,4,7,10,13-Pentaoxa-16-azacyclooctadecan-16-yl)-3-(2-methoxyethoxy)benzaldehyde (2). $POCl_3$ (3.72 mL, 40 mmol) was added dropwise to a vigorously stirring portion of anhydrous DMF which was kept in an ice bath in a N_2 atmosphere. The resulting pale yellow solution was stirred at room temperature for an additional 15 min. To this mixture, a DMF (2 mL) solution of 16-(2-(2-methoxyethoxy)phenyl)-aza-18-crown-6 **1** (ref. 42) (1.65 g, 4 mmol) was then slowly introduced and the resulting dark red solution was heated at 70 °C for 3 h. The reaction was cooled to room temperature, and poured into an an ice-cold satd $NaHCO_3$ solution. The mixture was extracted with 3 × 100 mL DCM/toluene (2 : 1) and dried over anhydrous $MgSO_4$. The solvent was evaporated *in vacuo* and the compound was purified by silica gel flash column chromatography (FCC) using DCM : MeOH (19 : 1) as the eluent and aldehyde **2** was obtained as a dark red oil (820 mg, 44% yield) ^{1}H NMR (400 MHz, $CDCl_3$) δ (ppm): 9.48 (s, 1H), 7.38 (d, 2H, $J = 7.5$ Hz), 7.17 (d, 2H, $J = 1.5$ Hz), 6.47 (dd, 2H, $J = 7.5, 1.5$ Hz), 4.31 (t, 2H, $J = 8.2$ Hz), 3.77 (d, 2H, $J = 8.2$ Hz), 3.60–3.52 (m, 24H), 3.41 (s, 3H). ^{13}C NMR (101 MHz, $CDCl_3$) δ (ppm): 191.01, 162.72, 148.11, 127.08, 122.39, 115.44, 115.09, 72.21, 69.01, 59.79, 59.12. LCMS calcd for $C_{22}H_{35}NO_8$ $[M + H]^+$ 442.24, found 442.19.

9-(4-(1,4,7,10,13-Pentaoxa-16-azacyclooctadecan-16-yl)-3-(2-methoxyethoxy)phenyl)-6-hydroxy-3H-xanthen-3-one (3). Aldehyde **2** (150 mg, 0.34 mmol, 1 equiv.) and resorcinol (82 mg, 0.74 mmol, 2.2 equiv.) were dissolved in 4.25 mL of trifluoroacetic acid (TFA) in a 35 mL pressure flask. The solution was then stirred at 115 °C for 13 h and concentrated by rotary evaporation to yield a crude red oil. The red oil was taken up in a silica column for purification by flash column chromatography (50% MeCN/toluene) to yield **3** (35 mg, 18% yield) as a bright yellow solid. ^{1}H NMR (400 MHz, $CDCl_3$) δ (ppm): 7.33 (d, 2H, $J = 7.3$ Hz), 6.84 (d, 2H, $J = 1.8$ Hz), 6.47–6.11 (m, 7H), 4.31 (t, 2H, $J = 8.2$ Hz), 3.77 (d, 2H, $J = 8.2$ Hz), 3.60–3.52 (m, 24H), 3.41 (s, 3H). ^{13}C NMR (101 MHz, $CDCl_3$) δ (ppm): 185.70, 162.72, 161.51, 155.92, 148.11, 127.08, 122.39, 115.44, 115.09, 95.73, 72.21, 69.01, 59.79, 59.12. LRMS calcd for $C_{34}H_{41}N O_{10}$ $[M + H]^+$ 624.70, found 624.49.

9-(4-(1,4,7,10,13-Pentaoxa-16-azacyclooctadecan-16-yl)-3-(2-methoxyethoxy)phenyl)-3-oxo-3H-xanthen-6-yl trifluoromethanesulfonate (4). **3** (414 mg, 1 mmol) was suspended in MeCN (10 mL). *N*-Phenyl-bis(trifluoromethane) sulfonimide (1.071 g, 3 mmol) was then added and the solution was allowed to stir for 3 h at room temperature. The solution was then evaporated and the crude compound was purified by column chromatography (silica gel, 5–20% MeOH in DCM) to afford **4** as a transparent light yellow oil (433 mg, 0.57 mmol, 57%) ^{1}H NMR (400 MHz, $CDCl_3$): δ 7.20–7.12 (m, 2H), 6.89–6.30 (m, 6H), 6.21 (d, 1H, $J = 1.6$ Hz), 4.31 (t, 2H, $J = 6.4$ Hz), 3.77 (t, 2H, $J = 6.4$ Hz), 3.64–3.54 (m, 24H), 3.35 (s, 3H). ^{13}C NMR (101 MHz, $CDCl_3$): δ 156.46, 149.93, 145.99, 134.71, 128.82, 125.07, 124.30,

123.97, 123.76, 115.57, 72.54, 70.42, 69.08, 61.84, 55.35, 49.43. LRMS calcd for $C_{35}H_{40}F_3NO_{12}S$ $[M + H]^+$ 755.76; found: 755.70.

***tert*-Butyl-4-(9-(4-(1,4,7,10,13-pentaoxa-16-azacyclooctade-can-16-yl)-3-(2-methoxyethoxy)phenyl)-3-oxo-3*H*-xanthen-6-yl) piperazine-1-carboxylate (5).** Compound **4** (433 mg, 0.57 mmol), BINAP (124 mg, 0.20 mmol), and palladium acetate (11 mg, 0.05 mmol) were suspended in THF (5 mL) and stirred at room temperature. 1-Boc-piperazine (279, 1.5 mmol) was then added and the solution was refluxed in a nitrogen atmosphere over-night. The reaction was then allowed to cool and filtered. The filtrate was evaporated and subjected to silica gel chromatog-raphy (40–100% EtOAc in hexanes) to yield **5** as a tan oil (214 mg, 0.26, 46%). ^{1}H NMR (400 MHz, CDCl$_3$): δ 7.22 (m, 2H), 6.82–6.30 (m, 7H), 6.21 (d, 1H, J = 1.6 Hz), 4.31 (t, 2H, J = 6.4 Hz), 3.77 (t, 2H, J = 6.4 Hz), 3.64–3.54 (m, 24H), 3.35 (s, 3H), 3.32–3.29 (m, 8H), 1.41 (s, 9H). ^{13}C NMR (101 MHz, CDCl$_3$): δ 164.25, 157.24, 152.89, 152.51, 141.87, 139.99, 137.24, 135.91, 134.98, 132.44, 131.21, 130.74, 130.39, 124.57, 122.88, 67.21, 62.46, 56.49, 28.01, 20.85. LRMS calcd for $C_{38}H_{50}N_3O_{15}$ $[M + H]^+$ 791.46; found: 791.5.

9-(4-(1,4,7,10,13-Pentaoxa-16-azacyclooctadecan-16-yl)-3-(2-methoxyethoxy)phenyl)-6-(piperazin-1-yl)-3*H*-xanthen-3-one (6). Compound **5** was dissolved in 5 mL of DCM. 5 mL of TFA was added to the solution in a nitrogen atmosphere. The mixture was stirred for 5 h at ambient temperature. The resulting solution was evaporated under reduced pressure to yield a dark brown oil crude product (198 mg). The crude product **6** was used for the following step without purification.

Methyl 2-(4-(9-(4-(1,4,7,10,13-pentaoxa-16-azacyclooctade-can-16-yl)-3-(2-methoxyethoxy)phenyl)-3-oxo-3*H*-xanthen-6-yl) piperazin-1-yl)acetate (7). Compound **6** from the previous deprotection step was dissolved in 5 mL of dry MeCN. Methyl bromoacetate (141 μL, 1.5 mmol) and sodium carbonate (742 mg, 7 mmol) were then added and the solution was refluxed for 13 h. After 13 h, the mixture was cooled down to ambient temperature and poured into water (50 mL) and then extracted with ethyl acetate (3 × 50 mL). The combined organic layers were dried over sodium sulfate, filtered and concentrated *via* rotary evaporation. The crude residue was purified using flash chromatography (silica gel, 0–20% MeOH in DCM) to yield **7** as a foamy brown solid (93 mg, 0.12 mmol) ^{1}H NMR (400 MHz, CD$_3$CN): δ 7.35 (m, 2H), 6.99–6.37 (m, 7H), 6.28 (d, 1H, J = 1.4 Hz), 4.31 (t, 2H, J = 6.7 Hz), 3.77 (t, 2H, J = 6.7 Hz), 3.64–3.54 (m, 27H), 3.37–3.29 (m, 7H), 3.22 (s, 2H), 2.51 (t, 4H, J = 5.3 Hz). ^{13}C NMR (101 MHz, CD$_3$CN): δ 166.42, 147.65, 145.88, 141.95, 137.27, 133.71, 131.64, 124.21, 123.71, 119.45, 112.76, 110.76, 109.81, 107.97, 107.79, 79.96, 70.36, 70.33, 69.58, 69.47, 55.63, 55.47, 43.18, 42.73, 28.36. LC-MS calculated for $C_{37}H_{41}BrN_4O_{14}S_2Na$ $[M + Na^+]$: 763.11; found: 763.31.

Potassium Sensor 525, PS525, (8). Compound **7** (50 mg, 0.06 mmol) was suspended in 5 mL of THF. Then 5 mL of 1 M LiOH solution was added slowly to the above mixture while stirring. After 1 h of stirring, the mixture had become homogeneous. After 24 h, the solution was put in an ice bath and 2 mL of 3 M HCl was added, and the mixture was allowed to warm to room temperature. Following the addition of 20 mL of saturated aqueous NaCl solution, the mixture was extracted four times

with 10 mL portions of EtOAc, and the combined organic layers were evaporated. Purification by high-performance liquid chromatography (Agilent) on a C18 column using a linear gradient of 20–100% CH$_3$CN over 50 minutes gave **PS525** as a light-yellow powder (23 mg, 0.03 mmol, 48%). ^{1}H NMR (400 MHz, CD$_3$CN): δ 7.35 (m, 2H), 6.99–6.37 (m, 7H), 6.28 (d, 1H, J = 1.4 Hz), 4.31 (t, 2H, J = 6.7 Hz), 3.77 (t, 2H, J = 6.7 Hz), 3.64–3.54 (m, 27H), 3.37–3.29 (m, 4H), 3.22 (s, 2H), 2.51 (t, 4H, J = 5.3 Hz). ^{13}C NMR (101 MHz, CD$_3$CN): δ 180.91, 176.99, 166.01, 147.32, 145.55, 141.72, 137.07, 133.21, 129.58, 123.97, 123.42, 119.03, 112.40, 110.36, 109.49, 107.48, 79.50, 70.02, 69.98, 69.22, 69.10, 55.27, 71.03, 55.12, 42.83, 42.40, 28.07. HRMS-ESI calculated for $C_{41}H_{53}N_3O_{11}$ $[M + H^+]$: 750.1757; found: 750.1764.

Ratiometric Potassium Sensor-1, RPS-1. PS525 (21 mg, 0.03 mmol), compound **9** (ref. 63) (19 mg, 0.06 mmol), and TATU (32 mg, 0.10 mmol) were dissolved in 2 mL of dry DMF and stirred in a nitrogen atmosphere. DBU was then added to the solution. The reaction was kept at room temperature for 12 h. Purification by high-performance liquid chromatography (Agi-lent) was carried out on a C18 column using a linear gradient of 40–100% CH$_3$CN over 50 min. Fractions containing the product were combined, evaporated under vacuum and lyophilized to give **RPS-1** as a brown powder (11.7 mg, 0.014 mmol, 48%). ^{1}H NMR (400 MHz, CD$_3$CN): δ 8.32 (s, 1H), 7.35 (m, 2H), 7.28 (s, 1H), 6.99–6.37 (m, 7H), 6.28 (d, 1H, J = 1.4 Hz), 4.31 (t, 2H, J = 6.7 Hz), 4.13 (t, 2H, J = 6.2 Hz), 3.97 (t, 2H, J = 5.8 Hz), 3.77 (t, 2H, J = 6.7 Hz), 3.64–3.54 (m, 27H), 3.37–3.29 (m, 8H), 3.22 (s, 2H), 2.79 (m, 4H), 2.51 (t, 4H, J = 5.3 Hz), 1.81–1.60 (m, 8H) ^{13}C NMR (101 MHz, CD$_3$CN): δ 180.93, 177.26, 166.42, 155.72, 153.70, 147.65, 145.88, 141.95, 137.27, 136.07, 133.21, 124.21, 123.71, 119.45, 112.76, 110.76, 109.81, 107.97, 107.79, 79.96, 70.36, 70.33, 69.58, 69.47, 59.54, 55.63, 55.47, 52.48, 51.23, 43.18, 42.73, 28.36, 26.17, 25.91, 23.01. HRMS-ESI calculated for $C_{40}H_{51}N_3O_{11}$ Na $[M + Na^+]$: 771.1142; found: 771.1183.

Spectroscopic methods

Fluorescence turn-on responses to potassium. Two different 50 mM HEPES (pH 7.4) solutions, solution A and solution B were made. Solution A contained 200 mM Na$^+$ and solution B contained 200 mM K$^+$. Solution A and B were mixed in different ratios to yield 1 mL final buffer solution with 0, 5, 10, 20, 30, 40, 50, 70, 90, 110, 130, 150, 200 mM respectively. A 2 μM solution of **PS525** was prepared by diluting 1 mM DMSO stock solution of **PS525** with each buffer in a 1 : 500 ratio into a 1 cm × 1 cm capped quartz cuvette. The probe solution was incubated at 37 °C for 5 minutes. Emission spectra were collected for **PS525** (λ_{ex} = 525 nm, λ_{em} = 545–700 nm).

Metal selectivity experiments. A 2 μM solution of **PS525** was prepared by diluting a 1 mM DMSO stock solution of the probe into 1 mL 50 mM HEPES (pH 7.4). 500 μL aliquots of this solution were added to ten 1 cm × 1 cm capped quartz cuvettes and then 500 μL of the metal of interest was added to the cuvette to bring the concentration of transition metals to 10 μM and with the exception of Na$^+$ at 5 mM. The emission spectrum was then recorded for each metal of interest solution.

Preparation and staining of cell cultures. All cells were maintained at exponential growth as a monolayer in Dulbeco's Modified Eagle Medium (DMEM, Invitrogen). Cells were supplemented with 10% fetal bovine serum (FBS, Hyclone) and incubated at 37 °C in 5% CO_2. Cells were plated in phenol red-free medium on borosilicate chamber slides (Nunc) and allowed to grow to 60% confluence 1 day prior to imaging. Cells were stained by incubating a 10 μM solution of **RPS-1** in DMEM for 2 h. For the valinomycin-induced K^+ efflux experiments, the DMEM media was exchanged out for phosphate buffered metal solution (PBS, pH 7.4, M = Na or K such that $[Na + K]_{tot} = 160$ mM) containing 10 μM valinomycin (Invitrogen). The cells were allowed to equilibrate in the new media for 1 min prior to imaging.

ICP-MS. Cells were then rinsed twice with ice-cold potassium free buffer (150 mM Na^+ in 50 mM HEPES buffer, pH = 7.4), followed by the addition of 215 μL of concentrated nitric acid (BDH Aristar Ultra). The plates were sealed with Parafilm and incubated on a shaker overnight. Samples (150 μL) were further diluted in 2 mL of 2% nitric acid (made freshly from concentrated nitric acid and Milli-Q water) in 15 mL tubes (Sarstedt) and analyzed on a Thermo Fisher iCAP Qc ICP mass spectrometer in kinetic energy discrimination (KED) mode against a standard curve of known potassium and phosphorus concentrations (CMS-5, Inorganic Ventures), with Ga (20 μg L^{-1}, Inorganic Ventures) as an internal standard. Each experiment was carried out twice, and each condition was repeated in at least triplicate.

Confocal microscopy imaging. Microscopy experiments were performed using a Zeiss laser scanning microscope (model 710) equipped with a 40× water objective lens and 2010 Zeiss software (Carl Zeiss). Cells were imaged in a 37 °C stage incubator connected to 5% CO_2 gas inlet to buffer the media. The focal plane with the highest fluorescence was selected for each field of cells. Fields of cells were sampled from the bright field images only. Replicating experiments were conducted with different plates of cells.

Conflicts of interest

There are no conflicts to declare.

Acknowledgements

Notes and references

1 M. C. D'Adamo, L. Catacuzzeno, G. Di Giovanni, F. Franciolini and M. Pessia, *Front. Cell. Neurosci.*, 2013, 7, 1–21.

2 B. F. Palmer, *Clin. J. Am. Soc. Nephrol.*, 2014, 10, 1050–1060.

3 D. A. Baylor and J. G. Nicholls, *J. Physiol.*, 1969, 203, 555–569.

4 A. A. Grace and B. S. Bunney, *J. Neurosci.*, 1984, 4, 2877–2890.

5 D. L. Fortin, M. R. Banghart, T. W. Dunn, K. Borges, D. A. Wagenaar, Q. Gaudry, M. H. Karakossian, T. S. Otis, W. B. Kristan, D. Trauner and R. H. Kramer, *Nat. Methods*, 2008, 5, 331–338.

6 P. M. Hudgins and G. B. Weiss, *J. Pharmacol. Exp. Ther.*, 1968, 159, 91–97.

7 C. Juel, *Pfluegers Arch.*, 1986, 406, 458–463.

8 M. J. Bia and R. A. DeFronzo, *Am. J. Physiol.*, 1981, 240, F257–F268.

9 E. Féraille and A. Doucet, *Physiol. Rev.*, 2001, 81, 345–418.

10 N. M. Storey, J. P. O'Bryan and D. L. Armstrong, *Curr. Biol.*, 2002, 12, 27–33.

11 J. M. Burnell, B. H. Scribner, B. T. Uyeno and M. F. Villamil, *J. Clin. Invest.*, 1956, 35, 935–939.

12 C. Tian, R. Zhu, L. Zhu, T. Qiu, Z. Cao and T. Kang, *Chem. Biol. Drug Des.*, 2014, 83, 1–26.

13 L. Ge, N. T. Hoa, Z. Wilson, G. Arismendi-Morillo, X. T. Kong, R. B. Tajhya, C. Beeton and M. R. Jadus, *Int. Immunopharmacol.*, 2014, 22, 427–443.

14 A. Felipe, R. Vicente, N. Villalonga, M. Roura-Ferrer, R. Martínez-Mármol, L. Solé, J. C. Ferreres and E. Condom, *Cancer Detect. Prev.*, 2006, 30, 375–385.

15 H. Wulff, N. A. Castle and L. A. Pardo, *Nat. Rev. Drug Discovery*, 2009, 8, 982–1001.

16 S. A. Salyer, J. R. Olberding, A. A. Distler, E. D. Lederer, B. J. Clark, N. A. Delamere and S. J. Khundmiri, *Biochim. Biophys. Acta, Mol. Basis Dis.*, 2013, 1832, 1734–1743.

17 D. Urrego, A. P. Tomczak, F. Zahed, W. Stühmer, L. A. Pardo and W. Stuehmer, *Philos. Trans. R. Soc., B*, 2014, 2014, 1–9.

18 X. Huang and L. Y. Jan, *J. Cell Biol.*, 2014, 206, 151–162.

19 L. Leanza, E. Venturini, S. Kadow, A. Carpinteiro, E. Gulbins and K. A. Becker, *Cell Calcium*, 2015, 58, 1–8.

20 L. Leanza, M. Romio, K. A. Becker, M. Azzolini, L. Trentin, A. Managò, E. Venturini, A. Zaccagnino, A. Mattarei, L. Carraretto, A. Urbani, S. Kadow, L. Biasutto, V. Martini, F. Severin, R. Peruzzo, V. Trimarco, J. H. Egberts, C. Hauser, A. Visentin, G. Semenzato, H. Kalthoff, M. Zoratti, E. Gulbins, C. Paradisi and I. Szabo, *Cancer Cell*, 2017, 31, 516–531.e10.

21 E. K. Breuer, D. Fukushiro-Lopes, A. Dalheim, M. Burnette, J. Zartman, S. Kaja, C. Wells, L. Campo, K. J. Curtis, R. Romero-Moreno, L. E. Littlepage, G. L. Niebur, K. Hoskins, M. I. Nishimura and S. Gentile, *Cell Death Dis.*, 2019, 10, 1–15.

22 C. D. Bortner, F. M. Hughes and J. A. Cidlowski, A Primary Role for K and Na Efflux in the Activation of Apoptosis, *J. Biol. Chem.*, 1997, 272, 32436–32442.

23 F. M. Hughes, C. D. Bortner, G. D. Purdy and J. A. Cidlowski, *J. Biol. Chem.*, 1997, 272, 30567–30576.

24 U. Fiedler and J. Růžička, *Anal. Chim. Acta*, 1973, 67, 179–193.

25 M. Jospin, M. C. Mariol, L. Ségalat and B. Allard, *J. Physiol.*, 2002, 544, 373–384.

26 H. Bischof, M. Rehberg, S. Stryeck, K. Artinger, E. Eroglu, M. Waldeck-Weiermair, B. Gottschalk, R. Rost, A. T. Deak,

T. Niedrist, N. Vujic, H. Lindermuth, R. Prassl, B. Pelzmann, K. Groschner, D. Kratky, K. Eller, A. R. Rosenkranz, T. Madl, N. Plesnila, W. F. Graier and R. Malli, *Nat. Commun.*, 2017, **8**, 1–11.

27 T. T. Ruckh, C. G. Skipwith, W. Chang, A. W. Senko, V. Bulovic, P. O. Anikeeva and H. A. Clark, *ACS Nano*, 2016, **10**, 4020–4030.

28 C. H. Lee, J. Folz, W. Zhang, J. Jo, J. W. Y. Tan, X. Wang and R. Kopelman, *Anal. Chem.*, 2017, **89**, 7943–7949.

29 R. Wang, X. Du, Y. Wu, J. Zhai and X. Xie, *ACS Sens.*, 2018, **3**, 2408–2414.

30 Y. Shen, S. Y. Wu, V. Rancic, A. Aggarwal, Y. Qian, S. I. Miyashita, K. Ballanyi, R. E. Campbell and M. Dong, *Commun. Biol.*, 2019, **2**, 1–10.

31 M. P. Jewell, M. D. Greer, A. L. Dailey and K. J. Cash, *ACS Sens.*, 2020, **5**, 474–480.

32 R. Y. Tsien, *Fluorescent Probes of Cell Signaling*, 1989.

33 D. W. Domaille, E. L. Que and C. J. Chang, *Nat. Chem. Biol.*, 2008, **4**, 168–175.

34 K. P. Carter, A. M. Young and A. E. Palmer, *Chem. Rev.*, 2014, **114**, 4564–4601.

35 S. C. Dodani, A. Firl, J. Chan, C. I. Nam, A. T. Aron, C. S. Onak, K. M. Ramos-Torres, J. Paek, C. M. Webster, M. B. Feller and C. J. Chang, *Proc. Natl. Acad. Sci. U. S. A.*, 2014, **111**, 16280–16285.

36 C. M. Ackerman, S. Lee and C. J. Chang, *Anal. Chem.*, 2017, **89**, 22–41.

37 J. L. Kolanowski, F. Liu and E. J. New, *Chem. Soc. Rev.*, 2018, **47**, 195–208.

38 H. He, M. A. Mortellaro, M. J. P. Leiner, R. J. Fraatz and J. K. Tusa, *J. Am. Chem. Soc.*, 2003, **125**, 1468–1469.

39 F. He, Y. Tang, S. Wang, Y. Li and D. Zhu, *J. Am. Chem. Soc.*, 2005, **127**, 12343–12346.

40 S. Nagatoishi, T. Nojima, B. Juskowiak and S. Takenaka, *Angew. Chem.*, 2005, **117**, 5195–5198.

41 X. Fan, H. Li, J. Zhao, F. Lin, L. Zhang, Y. Zhang and S. Yao, *Talanta*, 2012, **89**, 57–62.

42 S. Ast, T. Schwarze, H. Müller, A. Sukhanov, S. Michaelis, J. Wegener, O. S. Wolfbeis, T. Körzdörfer, A. Dürkop and H. J. Holdt, *Chem.–Eur. J.*, 2013, **19**, 14911–14917.

43 X. Kong, F. Su, L. Zhang, J. Yaron, F. Lee, Z. Shi, Y. Tian and D. R. Meldrum, *Angew. Chem., Int. Ed.*, 2015, **54**, 12053–12057.

44 B. Sui, X. Yue, M. G. Tichy, T. Liu and K. D. Belfield, *Eur. J. Org. Chem.*, 2015, **2015**, 1189–1192.

45 G. Song, R. Sun, J. Du, M. Chen and Y. Tian, *Chem. Commun.*, 2017, **53**, 5602–5605.

46 K. Meuwis, N. Boens, F. C. De Schryver, J. Gallay and M. Vincent, *Biophys. J.*, 1995, **68**, 2469–2473.

47 P. Padmawar, X. Yao, O. Bloch, G. T. Manley and A. S. Verkman, *Nat. Methods*, 2005, **2**, 825–827.

48 W. Namkung, P. Padmawar, A. D. Mills and A. S. Verkman, *J. Am. Chem. Soc.*, 2008, **130**, 7794–7795.

49 R. D. Carpenter and A. S. Verkman, *Org. Lett.*, 2010, **12**, 1160–1163.

50 R. D. Carpenter and A. S. Verkman, *Eur. J. Org. Chem.*, 2011, **2011**, 1242–1248.

51 C. After, *Nat. Methods*, 2005, **2**, 5–8.

52 J. Yu, L. Zhang, X. Xu and S. Liu, *Anal. Chem.*, 2014, **86**, 10741–10748.

53 J. Huang, L. Ying, X. Yang, Y. Yang, K. Quan, H. Wang, N. Xie, M. Ou, Q. Zhou and K. Wang, *Anal. Chem.*, 2015, **87**, 8724–8731.

54 G. Grynkiewicz, M. Poenie and R. Y. Tsien, *J. Biol. Chem.*, 1985, **260**, 3440–3450.

55 A. T. Aron, M. O. Loehr, J. Bogena and C. J. Chang, *J. Am. Chem. Soc.*, 2016, **138**, 14338–14346.

56 C. Y. S. Chung, J. M. Posimo, S. Lee, T. Tsang, J. M. Davis, D. C. Brady and C. J. Chang, *Proc. Natl. Acad. Sci. U. S. A.*, 2019, **116**, 18285–18294.

57 C. C. Woodroofe and S. J. Lippard, *J. Am. Chem. Soc.*, 2003, **125**, 11458–11459.

58 R. A. Schultz, B. D. White, D. M. Dishone, K. A. Arnold and G. W. Gokel, *J. Am. Chem. Soc.*, 1985, **107**, 6659–6668.

59 G. W. Gokel, L. J. Barbour, R. Ferdani and J. Hu, *Acc. Chem. Res.*, 2002, **35**, 878–886.

60 A. P. De Silva, H. Q. N. Gunaratne, T. Gunnlaugsson, A. J. M. Huxley, C. P. McCoy, J. T. Rademacher and T. E. Rice, *Chem. Rev.*, 1997, **97**, 1515–1566.

61 J. E. Whitaker, R. P. Haugland, D. Ryan, P. C. Hewitt, R. P. Haugland and F. G. Prendergast, *Anal. Biochem.*, 1992, **207**, 267–279.

62 T. Xiao, C. M. Ackerman, E. C. Carroll, S. Jia, A. Hoagland, J. Chan, B. Thai, C. S. Liu, E. Y. Isacoff and C. J. Chang, *Nat. Chem. Biol.*, 2018, **14**, 655–663.

63 C. C. Woodroofe, A. C. Won and S. J. Lippard, *Inorg. Chem.*, 2005, **44**, 3112–3120.

64 E. Lastraioli, L. Guasti, O. Crociani, S. Polvani, G. Hofmann, H. Witchel, L. Bencini, M. Calistri, L. Messerini, M. Scatizzi, R. Moretti, E. Wanke, M. Olivotto, G. Mugnai and A. Arcangeli, *Cancer Res.*, 2004, 606–611.

65 S. Z. Chen, M. Jiang and Y. S. Zhen, *Cancer Chemother. Pharmacol.*, 2005, **56**, 212–220.

66 Z. Zhou, V. R. Vorperian, Q. Gong, S. Zhang and C. T. January, *J. Cardiovasc. Electrophysiol.*, 1999, **10**, 836–843.

67 I. L. Camero, N. K. R. Smith, T. B. Pool and R. L. Sparks, *Cancer Res.*, 1980, **40**, 1493–1500.